

RANS-BASED NUMERICAL SIMULATION OF CAPTIVE MODEL TESTS IN SHALLOW WATER FOR THE DTC CONTAINER CARRIER

Y Liu, School of Naval Architecture, Ocean and Civil Engineering, Shanghai Jiao Tong University, Shanghai, China

Z J Zou, School of Naval Architecture, Ocean and Civil Engineering, State Key Laboratory of Ocean Engineering, Shanghai Jiao Tong University, Shanghai, China; Collaborative Innovation Center for Advanced Ship and Deep-Sea Exploration, Shanghai, China

L Zou, School of Naval Architecture, Ocean and Civil Engineering, Shanghai Jiao Tong University, Shanghai, China

SUMMARY

In very shallow water, the effect of depth restriction is very significant and dominates ship manoeuvrability. In this paper, numerical simulations of the viscous flow around a bare hull of the DTC container carrier manoeuvring in shallow water are conducted at model scale using the CFD software STAR CCM+. RANS-based simulations of static drift and pure sway tests at 20% UKC and two forward speeds are carried out considering the dynamic sinkage and trim as well as the tank wall effect. The hydrodynamic forces acting on the hull, as well as dynamic sinkage and trim are predicted and discussed. Compared with the model test data, time histories of the forces and moments obtained from numerical simulations show satisfactory agreement, while some discrepancies are found in the dynamic sinkage and trim simulations.

NOMENCLATURE

a	Surface area (m^2)
b	Breadth of ship (m)
B	Width of tank (m)
F	External body force (N)
H	Depth of water of tank (m)
I	Identity matrix (-)
p	Pressure (N/m^2)
R_T	Total resistance (N)
S_m	Blockage factor (-)
T	Ship's even keel static draft (m)
tr	Transpose of the matrix (-)
v	Velocity (m/s)
v_g	Mesh grid velocity (m/s)
V	A cell of volume (m^3)
$Y+$	Dimensionless wall distance (-)
α	Volume fraction (-)
Γ	Viscous stress (N/m^2)
μ_{eff}	Sum of the laminar μ and turbulence viscosities μ_t ($N\ s/m^2$)
ρ	Density of water (kg/m^3)
DFBI	Dynamic Fluid Body Interaction
RANS	Reynolds-averaged Navier Stokes
UKC	Under-Keel Clearance

1 INTRODUCTION

A ship manoeuvring in restricted waters usually experiences much larger hydrodynamic forces than in unrestricted waters due to the hydrodynamic interaction between the ship and the bottom/bank of the waterway. This hydrodynamic interaction has detrimental influence on ship manoeuvrability and may result in marine accidents such as collision or grounding. The ship experiences dynamic sinkage and trim (squat), notably in very shallow waters, due to the hydrodynamic forces acting on the hull. In addition to the squat, shallow water flows are

influenced by various factors such as free surface elevation, tank wall blockage, ship speed, bank geometry, unsteady flow features, water depth, etc. Therefore, to ensure a safe navigation it is of great importance to accurately predict the hydrodynamic force acting on the ship by taking the shallow water effect into account.

Traditionally, model tests, full scale trials and theoretical and semi-theoretical methods are used to predict the squat and the hydrodynamic force acting on a manoeuvring ship [1, 2]. Among several methods for manoeuvring prediction, static or dynamic planar motion mechanism (PMM) test is one of the most commonly used approaches. Captive model tests were executed and the shallow water effect on ship manoeuvring was discussed [3, 4]. Some free-running tests in shallow water were also presented [5, 6]. Furthermore, programs based on slender-body theory were used to model the hydrodynamic flow around ships in shallow water [7, 8].

Nowadays, with the rapid development of computer technique and Computational Fluid Dynamics (CFD) method, CFD-based numerical prediction of the hydrodynamic forces has become possible. Ship manoeuvring predictions by solving unsteady Reynolds-averaged Navier Stokes (RANS) equations have been presented in SIMMAN 2008 Workshop [9]. In addition to the deep water manoeuvres, SIMMAN 2014 Workshop also focused on ship manoeuvring in shallow water [10]. In the past, there were many studies regarding the simulation of static manoeuvres [11, 12] while the unsteady manoeuvres were not covered, the situation has been changed recently [5, 13-14]. Free-running tests such as zigzag and turning manoeuvres were numerically studied in reference [5]. Captive model tests were numerically simulated for different drift angles, water depth to draft ratios and ship speeds [15-18]. As presented by these investigations, shallow water effect can be simulated by CFD but still without enough accuracy, especially in the very shallow water condition with below 20% UKC.

To further investigate the interaction between a ship and the bottom of a shallow waterway, this paper uses the benchmark cases of a DTC container carrier, which are provided by Flanders Hydraulics Research (FHR) and Ghent University [19] for the 4th Conference on Manoeuvring in Shallow and Confined Water (MASH-CON2016). The benchmark model tests contain harmonic yaw and harmonic sway tests with the DTC at 20% UKC. In this paper, numerical simulations of the viscous flow around the DTC bare hull manoeuvring in shallow water are conducted at model scale using the CFD software STAR CCM+. RANS-based simulations of the static drift and pure sway tests at 20% UKC are carried out considering the dynamic sinkage and trim as well as the side walls of the towing tank as in the model tests. The effect of free surface elevation on the hydrodynamic forces is included by using the Volume of Fluid (VOF) method. The numerical results are compared with the benchmark data and the hydrodynamic characteristics of ship-to-bottom interaction are analyzed.

2 MATHEMATICAL FORMULATION

The governing equations are RANS equations which are closed by modeling the Reynolds stress tensor using SST $k-\omega$ turbulence model. Mean flow quantities near the wall are simulated according to an all Y^+ wall treatment where blended wall function is adopted. This approach is flexible because of its ability to handle a range of local mesh refinement levels near the wall. Cells with low Y^+ values are assumed to be properly resolved such that no wall treatment is necessary, while cells of $Y^+ > 30$ are treated as in the logarithmic region. Simulation of the viscous flow around the DTC hull is obtained through a finite volume discretization of the numerical domain. A VOF method is employed to capture the position of the phase interface between water and air. Equations are solved as an uncoupled system using a segregated flow solver which employs a SIMPLE algorithm for pressure-velocity coupling.

2.1 COORDINATE SYSTEMS

Considering the feature of the ship motion, three Cartesian coordinate systems are established, as shown in Fig.1. Definitions of the coordinate system are identical to those of the model tests in reference [19]. $O_0-X_0Y_0Z_0$ is the earth-fixed coordinate system. $O-XYZ$ is the body-fixed coordinate system whose origin locates at the intersection of water plane, central longitudinal plane and mid-ship section plane, with X -axis pointing to the bow and Y -axis pointing to the starboard. The reference coordinate system $O_1-X_1Y_1Z_1$ maintains a static position during the heave, pitch or yaw motion. It coincides with the body-fixed coordinate system at rest. Reference coordinate system is used in the present simulations and also in computing the ship hydrodynamics.

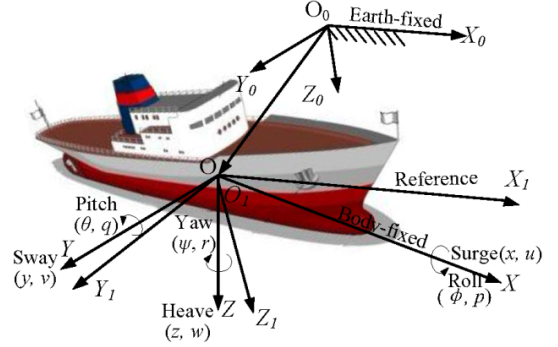


Figure 1. Coordinate systems in the simulation

2.2 GOVERNING EQUATIONS

The Navier-Stokes equations are given in the integral form as:

$$\frac{d}{dt} \int_V \rho dV + \oint_A \rho(\mathbf{v} - \mathbf{v}_g) \cdot d\mathbf{a} = 0 \quad (1)$$

$$\begin{aligned} \frac{d}{dt} \int_V \rho \mathbf{v} dV + \oint_A \rho \mathbf{v} \mathbf{x} (\mathbf{v} - \mathbf{v}_g) \cdot d\mathbf{a} = & - \oint_A p \mathbf{I} \cdot d\mathbf{a} \\ & + \oint_A \boldsymbol{\Gamma} \cdot d\mathbf{a} + \int_V \mathbf{F} dV \end{aligned} \quad (2)$$

The terms on the left hand side of Eq. (2) are the transient and convective flux terms respectively. Pressure gradient, viscous flux and body force terms are given on the right hand side.

The complete stress tensor for a turbulence flow invokes the Boussinesq approximation such that:

$$\boldsymbol{\Gamma} = \mu_{eff} [\nabla \mathbf{v} + \nabla \mathbf{v}^{tr} - \frac{2}{3} (\nabla \cdot \mathbf{v}) \mathbf{I}] \quad (3)$$

Turbulent viscosity is used to model the Reynolds stress tensor as a function of mean flow quantities so that the governing equations are closed.

A finite volume method (FVM) is used to discretize the flow domain as a finite number of control volumes (CVs) corresponding to computational grid cells. The formulation is with second-order accuracy in space and in time.

2.3 VOF INTERFACE CAPTURING

The air-water interface at the free surface is captured using the VOF method. VOF assumes a common velocity and pressure field for all phases within a single CV, and monitors the phase fraction. The governing equations for mass and momentum continuity in a single-phase flow are thus solved for an equivalent fluid whose physical properties (density and laminar viscosity) are a function of the constituent phase's properties and volume fractions within each CV. This is often known as the volume-fraction method. The transport of volume fraction is described by an additional conservation equation:

$$\frac{d}{dt} \int_V \alpha_i dV + \oint_A \alpha_i (\mathbf{v} - \mathbf{v}_g) \cdot d\mathbf{a} = 0 \quad (4)$$

3 NUMERICAL METHOD

3.1 SHIP MODEL

The geometry of DTC is shown in Fig. 2.



Figure 2. DTC geometry

In order to analyze the shallow water effect, FHR conducted captive model tests under 20% UKC as the very shallow water condition. L_{pp} is 355m and the designed draft T is 14.5m. The breadth of ship b is 51m. Other main particulars of the ship can be found in [20]. The dimension of FHR shallow water towing tank is 68.5m in effective length, 7.0m in width and 0.5m in maximum water depth. Sinkage and trim of DTC were free in the test, while roll of the hull was fixed.

3.2 COMPUTATIONAL DOMAIN AND GRIDS

The influences of tank side walls, squat, ship speed, drift angle, water depth are investigated in present computations. Both deep and shallow water simulations are conducted, their corresponding water depth to draft ratio are 10 and 1.2 respectively. Only straight-ahead and static drift motions are simulated in the static captive model tests under 20% UKC. For pure sway tests, two different forward speeds ($Fr=0.096$ and 0.139) under 20% UKC are considered. The corresponding Froude depth number Fr_h are 0.433 and 0.630. The amplitude and period of sway motion are 0.2m and 20s, respectively. Investigations of the effects of tank side walls and squat are conducted for the higher speed case ($Fr=0.139$).

Two domain widths are considered. The narrow domain width has the same value as in the towing tank, i.e. $1.757L_{pp}$, while the larger width is $5L_{pp}$. As shown in Fig. 3, the computational domain for all shallow water simulations extends $3.5L_{pp}$ from outlet plane to the A.P., $1.5L_{pp}$ from inlet plane to the F.P.. The bottom of the domain is determined according to the water depth considered. The boundary conditions shown in Fig. 3 are: velocity inlet for inlet plane, outflow for outlet plane, no slip condition for ship hull and slip condition for side walls. For the deep water case, slip condition on the bottom is used. In shallow water, however, the effect of the boundary layer on the bottom greatly influences the flow in the gap between the ship and the bottom, so a moving no-slip condition is used on the bottom.

An unstructured predominantly hexahedral mesh is applied in the computation. The grid is refined towards the free surface and the hull. Orthogonal prismatic cells are generated next to hull and bottom surface to improve the accuracy of the flow resolution. Prism layer is not used on the bottom surface in deep water case, where blockage effect is minor. Though different grids are used for simulating different captive model tests, the grid sizes

around the hull keep the same to minimize the influence of the grid fitness [16]. The grids consist of approximately 2.0M cells for the lower speed case ($Fr=0.096$). The Y^+ values are below 15. To avoid the negative volume during morphing (see Section 3.3), coarse grid is generated for higher speed and non-zero drift angle cases, which is about 1.5M cells. The Y^+ values are below 70. The grid structure around the ship and the bottom in shallow water is shown in Fig.4. The free surface, bow, stern as well as bottom parts are refined during mesh generation.

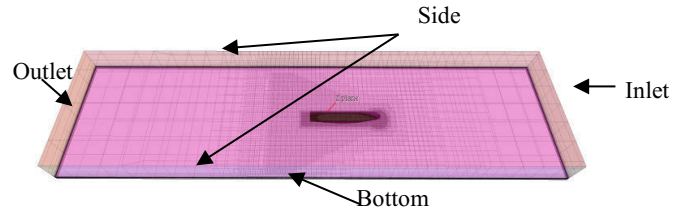


Figure 3. Computational domain and boundary with tank side walls in shallow water

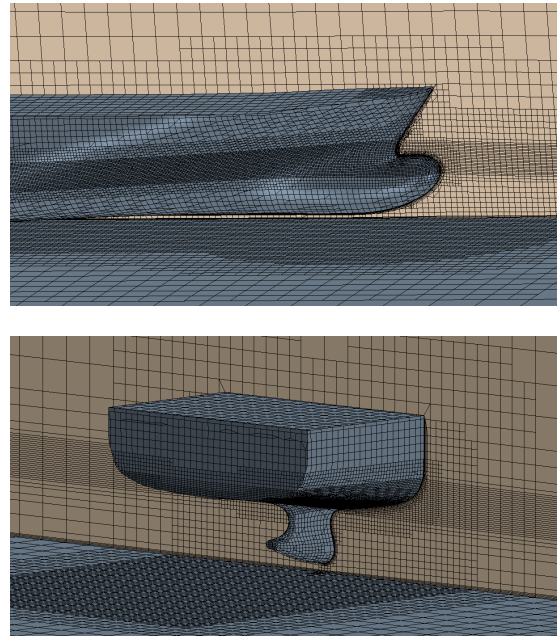


Figure 4. Mesh structure around ship and bottom in shallow water

3.3 DFBI MODULE

Dynamic Fluid Body Interaction (DFBI) module involves actual displacement of mesh vertices, which can model the motion of rigid bodies in six degrees of freedom (6-DOF) within the fluid system. 6-DOF Solver and 6-DOF Motion Solver model are then activated and used to compute the resultant fluid forces, gravitational forces and moments acting on the body caused by all influences, and solve the governing equations of rigid body motion to find its new position and orientation.

DFBI Translation and Rotation and DFBI morphing are used in this paper. The difference between these two

modules is that the former involves the whole mesh moving, while the latter uses control points and their associated displacements to generate an interpolation field throughout the region, which can then be used to displace the actual vertices of a mesh. “Six Dof Body” boundary and “Six Dof Body plus Displacement” are selected in DFBI morphing motion to trace the vertices on this boundary. User defined functions are written and added to the Field Function to define the additional specified displacement superposed in the 6-DOF body motion. All the simulations are carried out on a shared-memory workstation with 16 CPU cores (Intel XEON @ 2.60GHz).

4 RESULTS AND DISCUSSIONS

4.1 SIMULATIONS OF STATIC CAPTIVE MODEL TESTS IN DEEP AND SHALLOW WATER

4.1 (a) Validation of straight ahead test in deep water

In order to evaluate the accuracy of the numerical method, deep water case is simulated by two motion modules, i.e. DFBI Translation and Rotation and DFBI morphing. During all the simulations, sinkage and trim are free. The total resistance R_T of DTC hull under straight-ahead conditions is obtained and compared with the experimental data [20]. Table 1 shows the comparison between the CFD results and experimental data (EFD) at $Re=8.054 \times 10^6$ and $Fr=0.192$, where “E%D” denotes the relative error.

Table 1. Resistance results in deep water

Case*	R_T (N)	E%D (%)*
EFD	24.14	(-)
DFBI Translation and Rotation	25.146	4.1665
DFBI morphing	25.09	3.9373

* Ship model scale 1: 59.407

* E%D = (CFD-EFD)/ EFD \times 100%

From Table 1, it can be seen that both of these two numerical methods over-predict the resistance, but their relative errors are small and DFBI morphing method is slightly better. Because the method of DFBI Translation and Rotation cannot solve the near wall problem when considering squat, DFBI morphing method is selected for the following computations.

4.1 (b) Validation of static drift test in shallow water

In this section, straight-ahead ($\beta = 0^\circ$) and static drift ($\beta = 2.5^\circ$) motions are numerically simulated under 20% UKC. Modeling static drift motion in shallow water is more difficult comparing to the deep water case due to the blockage effects, and it is much more time-consuming. Fig. 5 shows the computed transient oscillation and the convergence of sinkage and trim in $\beta = 0^\circ$ case, where non-dimensional trim is obtained by dividing the difference in vertical position at the fore and aft

perpendiculars by L_{pp} . It can be seen that both sinkage and trim converge to an approximate constant value.

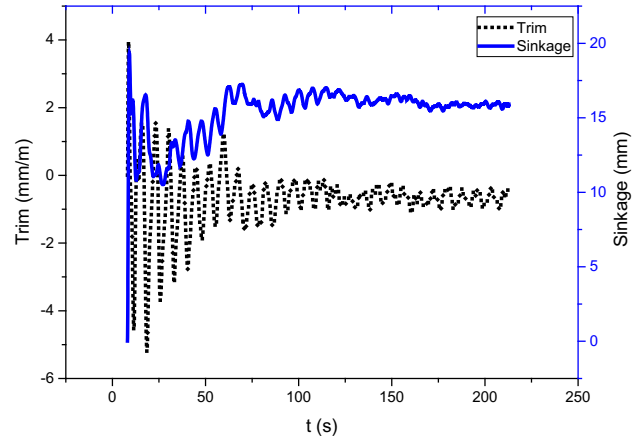


Figure 5. Transient oscillation and convergence of sinkage and trim in $\beta = 0^\circ$ case

Table 2 shows the computed results of sinkage and trim, as well as the relative error compared with the experimental data at $Fr=0.139$ ($Fr_h=0.630$). The error of trim is much larger than that of sinkage. More investigations are needed to find out the reason. When the drift angle turns to nonzero, both sinkage and trim are increased. Compared to the experimental data, the increase ratios of computational value are much smaller. Moreover, CFD computations under-predict the sinkage and trim under static drift ($\beta = 2.5^\circ$) conditions and sinkage under straight-ahead ($\beta = 0^\circ$) condition, but over-predict the trim under straight-ahead ($\beta = 0^\circ$) condition.

Table 2. Results and errors of sinkage and trim

Case*	Squat		E%D (%)	
	Trim (mm/m)	Sinkage (mm)	Trim (%)	Sinkage (%)
EFD- $\beta = 0^\circ$	-0.3886	16.4508	(-)	(-)
CFD- $\beta = 0^\circ$	-0.6540	15.9327	68.3	-3.15
EFD- $\beta = 2.5^\circ$	-2.0207	18.1347	(-)	(-)
CFD- $\beta = 2.5^\circ$	-0.7118	16.9858	-64.77	-6.335

* Ship model scale 1: 89.11

4.2 SIMULATIONS OF HARMONIC SWAY MODEL TESTS IN SHALLOW WATER

Pure sway tests are simulated with 0.05Hz frequency and 0.2m oscillation amplitude as shown in Fig. 6. The ship has a constant forward speed U along the towing tank and a periodically varying lateral displacement. The simulation starts when the hull position locates at tank centerline, while the experiment data is started to record when the hull turns to maximum lateral sway. In order to compare with the experiment directly, the computation in the first quarter of period is ignored. Furthermore, release time and ramp time in the computations are up to 20s to allow some time for the fluid flow to initialize.

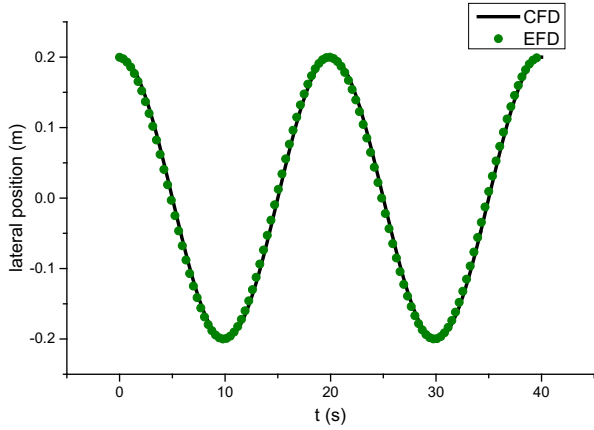


Figure 6. Pure sway (model scale 1: 89.11)

4.2 (a) $Fr_h=0.63$

In order to discuss how the squat and tank side walls affect the hydrodynamic forces in shallow water, four different cases are numerically simulated at $Fr_h=0.63$. The case definition and parameters are summarized in Table 3. Two domain widths and blockage factors S_m are listed there. Two kinds of ship states are considered. Dynamic ship squat is numerically simulated as model tests while fixed ship has zero sinkage and trim.

Table 3. Cases definition and parameters

Case No.	Domain	S_m	State	Sinkage	trim
1	wide	0.024	fixed	0	0
2	bank	0.069	fixed	0	0
3	wide	0.024	squat	dynamic	dynamic
4	bank	0.069	squat	dynamic	dynamic

$$S_m = (b \times T) / (B \times H)$$

Fig. 7-Fig. 9 show the hydrodynamic forces and moments of these four cases, as well as the comparison with the experimental data. These figures show that the hydrodynamic forces and moments obtained for Case 4 are the most accurate ones compared to the experimental data. When both ship squat and tank side walls are ignored (Case 1), the amplitudes of lateral force and yaw moment decrease by more than 50% compared with the results of Case 4. When comparing the results of Case 2 and Case 3 with those of Case 4, the amplitude of hydrodynamic forces and moment of Case3 is quantitatively larger than those of Case 2. It means that the squat plays a more important role in affecting hydrodynamic forces than the blockage effect by the tank side walls. In Case 4, CFD prediction gives the best results but still there are discrepancies. It under-predicts lateral force while over-predicts yaw moment at peak values.

Fig. 10 and Fig. 11 show the dynamic sinkage and trim during pure sway in 2 periods. For Case 4, the same trends of the sinkage and trim are predicted qualitatively

as in the tests, but with some error in value. Case 4 has a relative better trend than Case 3 since the time when the sinkage and trim value reaches extreme points in Case 4 basically coincides with experiment data. Nevertheless, the sinkage is much under-predicted compared with EFD data. The large errors in computations are probably caused by the coarse grid or the increased complexity of the flow. The experimental investigations do not show a fully steady state of ship's sinkage and trim neither. Since the error and uncertainty of the model test data are not available, it is difficult to draw any conclusion so far.

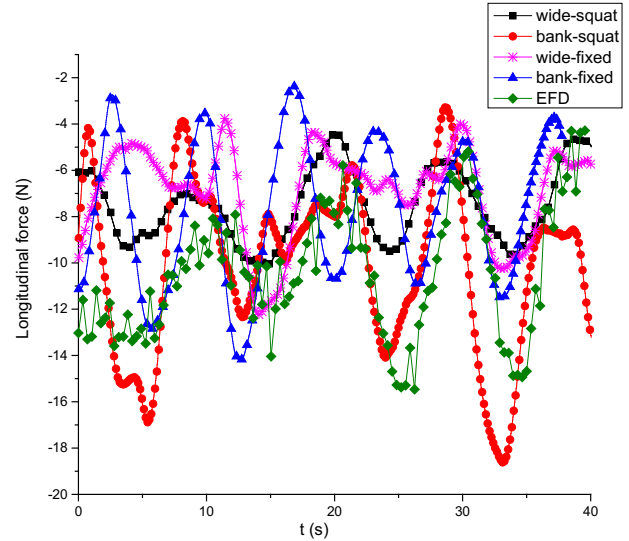


Figure 7. Time history of longitudinal force ($Fr_h=0.63$)

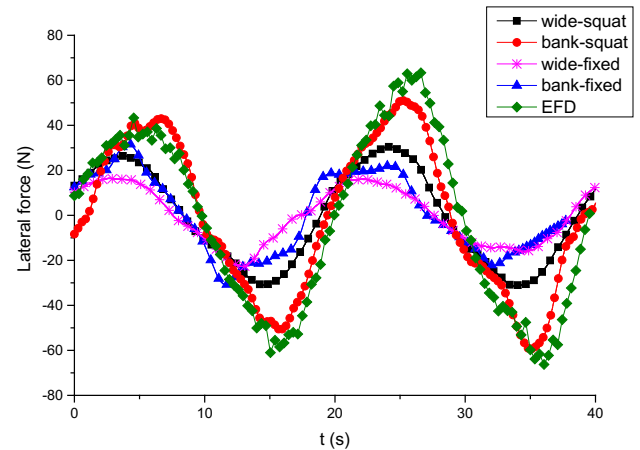


Figure 8. Time history of lateral force ($Fr_h=0.63$)

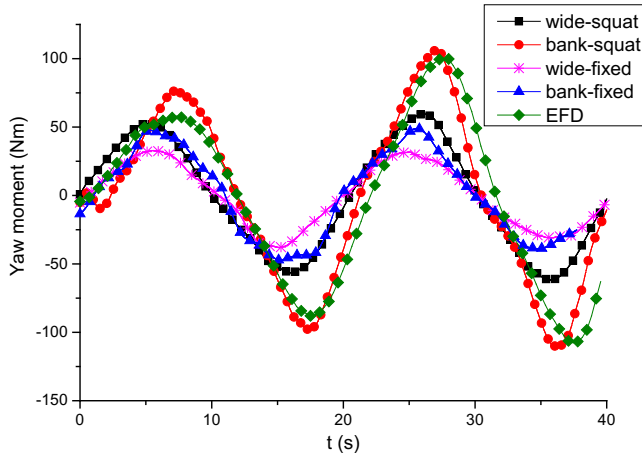


Figure 9. Time history of yaw moment ($Fr_h=0.63$)

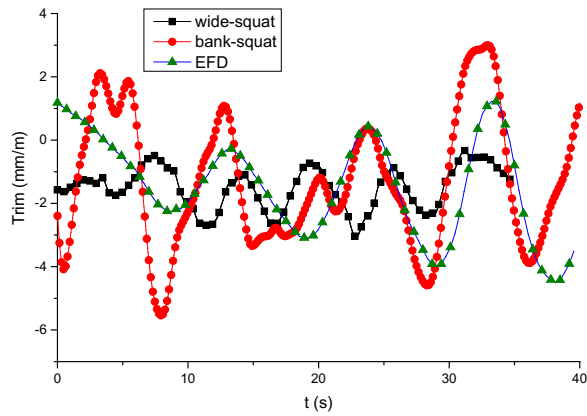


Figure 10. Time history of trim ($Fr_h=0.63$)

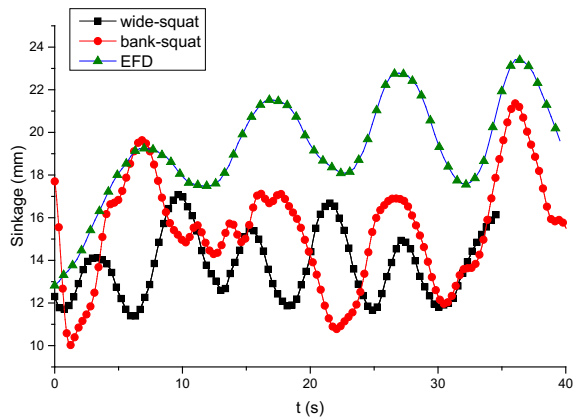
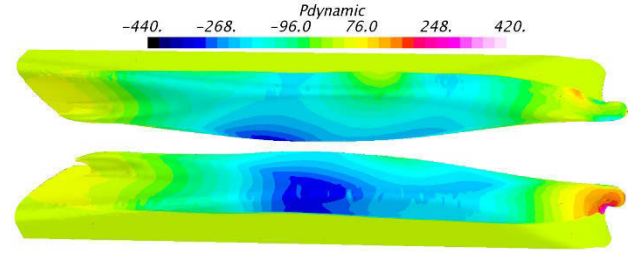
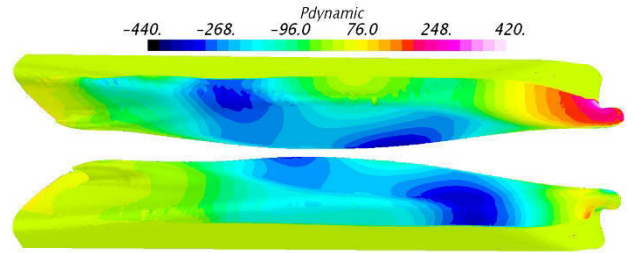


Figure 11. Time history of sinkage ($Fr_h=0.63$)

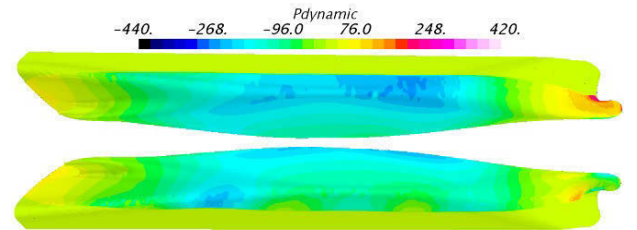
Fig. 12 shows the pressure contours on the hull at three successive motion phases: maximum lateral displacement to port (180°), central position of the tank (270°), and maximum lateral displacement to starboard (360°). Only Case 4 is considered for the comparison with lower Fr case to be discussed below. A strong port-starboard asymmetry of the pressure is observed on the hull according to Fig.12.



(a) Maximum lateral displacement to port (180°)



(b) Central position of the tank (270°)



(c) Maximum lateral displacement to starboard (360°)

Figure 12. Pressure contours at three successive motion phases ($Fr_h=0.63$)

4.2 (b) $Fr_h=0.433$

As shown in the last subsection, the tank side walls and squat have tremendous influences on the hydrodynamic characteristics in shallow water, so for pure sway case at $Fr_h=0.433$, only the conditions of Case 4 are considered in the computations.

The hydrodynamic forces and moment, as well as squat compared with EFD data are shown in Fig. 13-Fig. 17. The time histories of computed and measured lateral force and yaw moment are in good agreement. Although there are some discrepancies between computed and measured longitudinal force, sinkage and trim, their trends are reasonable to some extent. All the peak values are smaller than those of $Fr_h=0.63$, which means in addition to squat and tank side walls, ship speed is another important factor affecting the ship-bottom interaction.

Fig. 18 shows pressure contours on the hull at three successive motion phases: maximum lateral displacement to port (180°), central position of the tank (270°), and maximum lateral displacement to starboard (360°). Compared to the higher Fr_h , the whole pressure on the hull decreases. The pressure distribution of each phase shows slight differences.

Fig. 19 gives the vorticity contour from the port/starboard side view at two different ship velocities. Strong asymmetric bilge vortices around the hull are generated by the interactions with the side wall and bottom. When the ship speed increases, vorticity system looks similar but the strength is larger. Fig.12, Fig.18 and Fig 19 reveal the complexity of the turbulent flow in the pure sway motion in shallow waters.

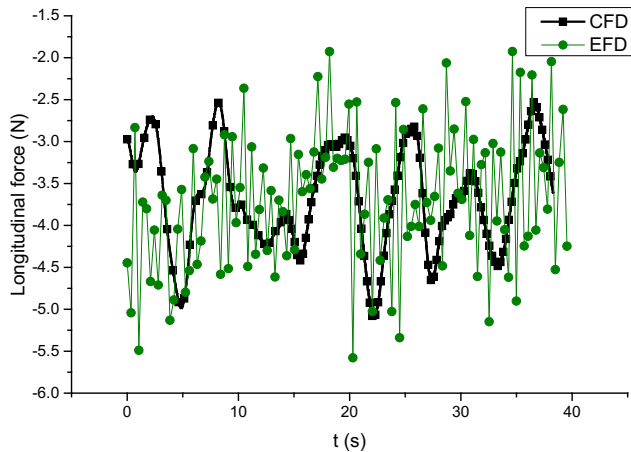


Figure 13. Time history of longitudinal force ($Fr_h=0.433$)

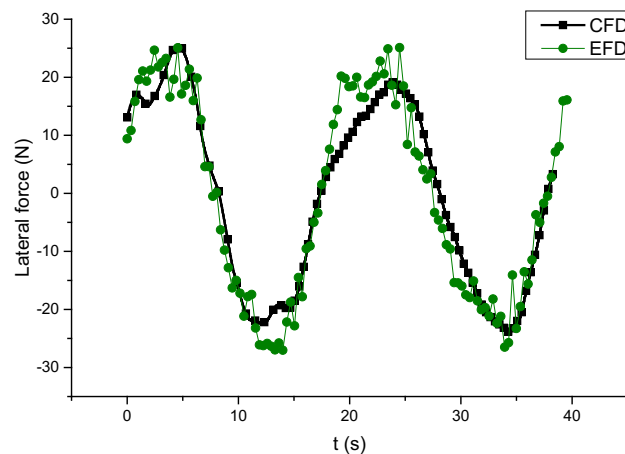


Figure 14. Time history of lateral force ($Fr_h=0.433$)

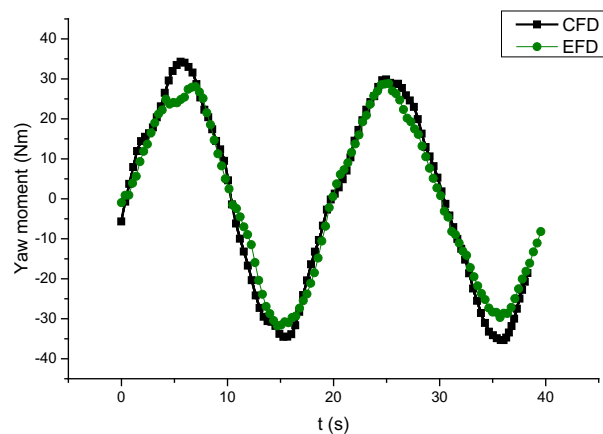


Figure 15. Time history of yaw moment ($Fr_h=0.433$)

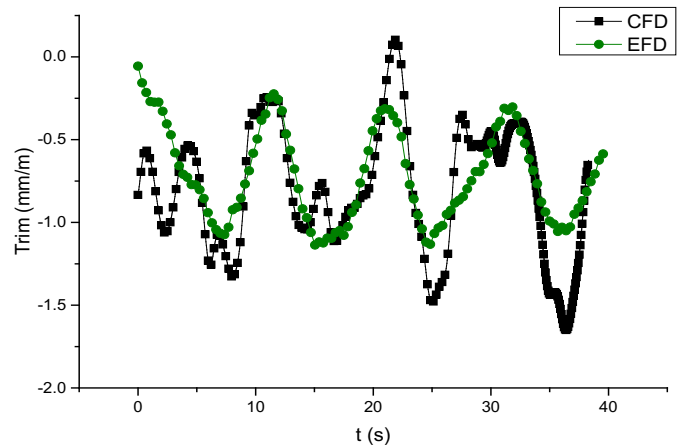


Figure 16. Time history of trim ($Fr_h=0.433$)

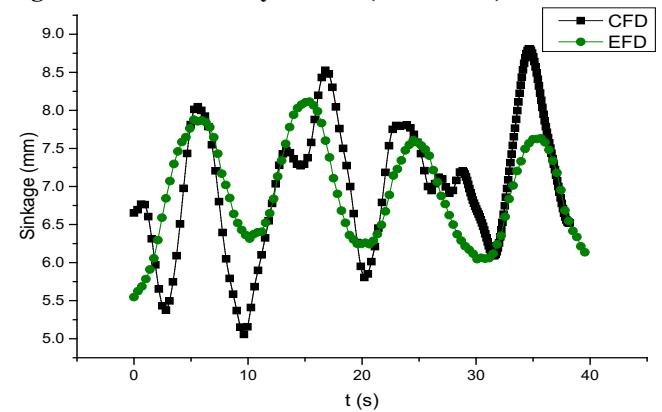
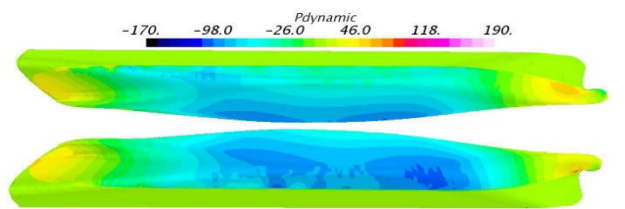
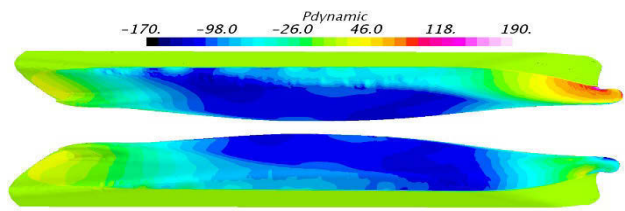


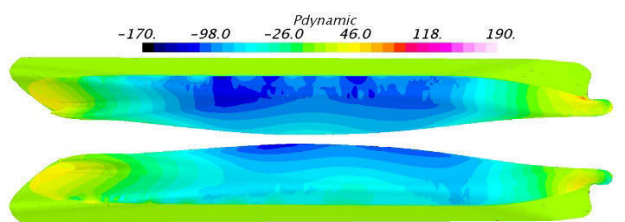
Figure 17. Time history of sinkage ($Fr_h=0.433$)



(a) Maximum lateral displacement to port (180°)

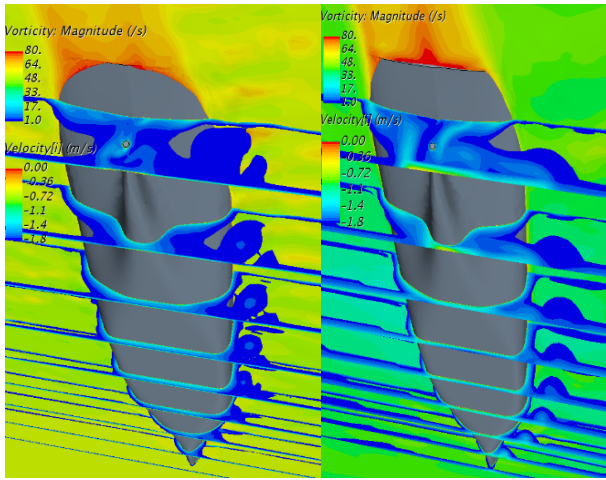


(b) Central position of the tank (270°)

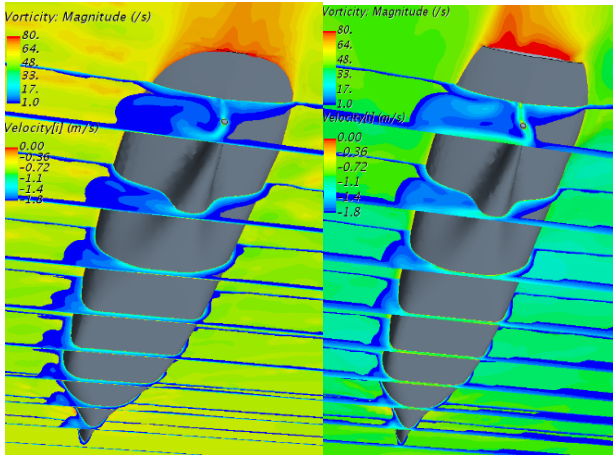


(c) Maximum lateral displacement to starboard (360°)

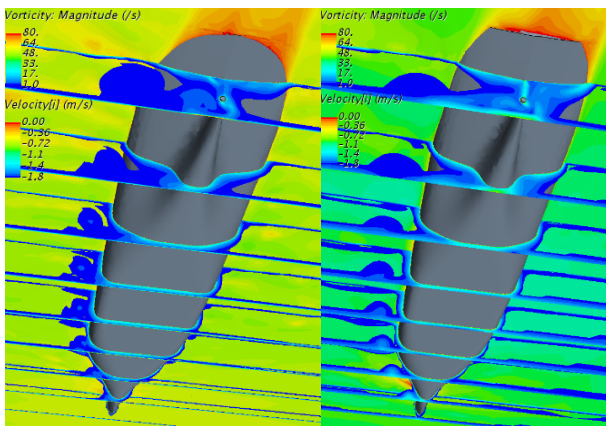
Figure 18. Pressure contours at three successive motion phases ($Fr_h=0.433$)



(a) Maximum lateral displacement to port (180°)



(b) Central position of the tank (270°)



(c) Maximum lateral displacement to starboard (360°)

Figure 19. Cross sections colored with vorticity magnitude at three successive motion phases. Free surface colored with velocity (Left: $Fr_h = 0.433$ Right: $Fr_h = 0.63$)

5 CONCLUSIONS

In this paper, RANS-based simulations of the static drift and pure sway tests of a DTC model at 20% UKC are carried out considering its dynamic sinkage and trim, as well as the effects of tank side walls at two forward speeds with $Fr_h = 0.63$ and $Fr_h = 0.433$. DFBI morphing method is adopted to simulate the dynamic sinkage and trim. The hydrodynamic forces acting on the hull, dynamic sinkage and trim under these conditions are predicted and discussed.

The numerical method applied in the present paper is validated by comparing the predicted resistance with EFD data in deep water. For shallow water computations, the squat, tank wall and ship speed are shown to be important and the results indicate that those factors greatly influence the transverse force, dynamic sinkage and trim. When considering tank side bank and ship squat, CFD prediction gives the best results compared with EFD data but still there are slight discrepancies. It under-predicts lateral force while over-predicts yaw moment at peak values with higher Fr number. Moreover, Details of simulated flow field, such as pressure distribution and vorticity around the hull are given to explain the hydrodynamic characteristics.

However, the computed sinkage and trim do not match the experimental data very well, especially at higher Fr number where the sinkage is under-predicted. Reasons for the discrepancies are still not clear. More studies are needed to investigate the error and to further improve the accuracy in the computations.

6 ACKNOWLEDGEMENTS

This work is supported by the National Natural Science Foundation of China (Grant No: 51309152).

7 REFERENCES

1. Briggs, M.J. (2006). *Ship squat predictions for ship/tow simulator*. DTIC Document.
2. Ankudinov, V.; Daggett, L.; Huval, C.; Hewlett, C. (1996). Squat predictions for manoeuvring applications. *Seventh International Conference on Marine Simulation and Manoeuvrability (MARSIM)*, Copenhagen, Denmark.: pp.467-495.
3. Maimun, A.; Priyanto, A.; Muhammad, A.; Scully, C.; Awal, Z. (2011). *Manoeuvring prediction of pusher barge in deep and shallow water*. in *Ocean Engineering*. pp. 1291-1299. doi: 10.1016/j.oceaneng.2011.05.011.
4. Eloit, K.; Marc, V.; Delefortrie, G. (2006). Prediction of ship manoeuvrability of an 8000 TEU containership in deep and shallow water: mathematical modelling and captive model testing.

- International Conference on Marine Simulation and Ship Manoeuvring (MARSIM)*, Terschelling, The Netherlands. pp.3-1.
5. Carrica, P.M.; Mofidi, A.; Eloot, K.; Delefortrie, G. (2016). Direct simulation and experimental study of zigzag maneuver of KCS in shallow water. *Ocean Engineering* 112: pp. 117-133. doi: 10.1016/j.oceaneng.2015.12.008.
 6. Tonelli, R.; Quadvlieg, F. (2015). New Benchmark Data for Manoeuvring in Shallow Water Based on Free Running Manoeuvring Tests Including Uncertainty of the Results. *Thirty-fourth International Conference on Ocean, Offshore and Arctic Engineering (OMAE)*, St. John's, Newfoundland, Canada.
 7. Gourlay, T.P. (2014). ShallowFlow: A Program to Model Ship Hydrodynamics in Shallow Water. *Thirty-third International Conference on Ocean, Offshore and Arctic Engineering (OMAE)*, San Francisco, California, USA. pp.V01AT01A018-V01AT01A018.
 8. Tuck, E. (1966). Shallow-water flows past slender bodies. *Journal of Fluid Mechanics* 26(01): pp. 81-95. doi: 10.1017/S0022112066001101.
 9. SIMMAN (2008). *Workshop on Verification and Validation of Ship Manoeuvring Simulation Methods*, Copenhagen, Denmark.
 10. SIMMAN (2014). *Workshop on Verification and Validation of Ship Manoeuvring Simulation Methods*, Copenhagen, Denmark.
 11. Van Hoydonck, W.; Eloot, K. (2014). Shallow water CFD computations for SIMMAN 2014. *Workshop on Verification and Validation of Ship Manoeuvring Simulation Methods (SIMMAN)*, Copenhagen, Denmark.
 12. Böttner, C.-U.; Kastens, M.; Hirata, N.; Wasserbau, B.F. (2014). Contribution to numerical Test Cases in shallow water conditions. *Workshop on Verification and Validation of Ship Manoeuvring Simulation Methods (SIMMAN)*, Copenhagen, Denmark.
 13. Liu, X.; Wan, D. (2015). Numerical Simulation of Ship Yaw Maneuvering in Deep and Shallow Water. *Twenty-fifth International Offshore and Polar Engineering Conference (ISOPE)*, Kona, Hawaii, USA.
 14. Liu, X.; Fan, S.; Wang, J.; Wan, D. (2015). Hydrodynamic Simulation of Pure Sway Tests with Ship Speed and Water Depth Effects. *Twenty-fifth International Offshore and Polar Engineering Conference (ISOPE)*, Kona, Hawaii, USA.
 15. Simonsen, C.; Stern, F.; Agdrup, K. (2006). CFD with PMM test validation for manoeuvring VLCC2 tanker in deep and shallow water. *International Conference on Marine Simulation and Ship Manoeuvring (MARSIM)*, Terschelling, The Netherlands.
 16. Toxopeus, S.; Simonsen, C.; Guilmineau, E.; Visonneau, M.; Xing, T.; Stern, F. (2013). Investigation of water depth and basin wall effects on KVLCC2 in manoeuvring motion using viscous-flow calculations. *Journal of Marine Science and Technology* 18(4): pp. 471-496. doi: 10.1007/s00773-013-0221-6.
 17. Koop, A. (2015). Shallow Water Current Loads on a LNG Carrier Using CFD. *Thirty-fourth International Conference on Ocean, Offshore and Arctic Engineering (OMAE)*, St. John's, Newfoundland, Canada. American Society of Mechanical Engineers.
 18. Toxopeus, S.L. (2013). Viscous-flow calculations for KVLCC2 in deep and shallow water. *Fourth International Conference on Computational Methods in Marine Engineering (MARINE)*, Netherlands. Springer: pp.151-169.
 19. Eloot, K.; Marc, V.; Guillaume, D.; Evert, L. (2016). Running Sinkage and Trim of the DTC Container Carrier in Harmonic Sway and Yaw Motion: Open Model Test Data for Validation Purposes. *Fourth International Conference on Ship Manoeuvring in Shallow and Confined Water (MASHCON): Ship - Bottom Interaction*, Hamburg, Germany (to be published).
 20. Moctar, O.E.; Shigunov, V.; Zorn, T. (2012). Duisburg Test Case: Post-panamax container ship for benchmarking. *Ship Technology Research* 59(3): pp. 50-64. doi: 10.1179/str.2012.59.3.004.

8 AUTHORS' BIOGRAPHIES

Yi Liu holds the current position of PhD student at School of Naval Architecture, Ocean and Civil Engineering, Shanghai Jiao Tong University. Her previous experience includes numerical studies on the ship manoeuvring in restricted waters, etc.

Zaojian Zou holds the current position of full professor at School of Naval Architecture, Ocean and Civil Engineering, Shanghai Jiao Tong University. He is responsible for teaching and research on marine hydrodynamics. His previous experience includes PI of some projects on manoeuvring and control of ships and other marine vehicles. He was a member of the 22nd, 23rd, 25th and 26th ITTC MC.

Lu Zou is a lecturer at School of Naval Architecture, Ocean and Civil Engineering, Shanghai Jiao Tong University. Her major research interest is in the ship manoeuvring in confined waters, as well as Verification and Validation of CFD simulations.